The structure of schwertmannite, a nanocrystalline iron oxyhydroxysulfate

A. Fernandez-Martinez,[1,2,*] V. Timon,[3] G. Roman-Ross,[4] G.J. Cuello,[2,5] J.E. Daniels,[6] and C. Ayora[7]

[1]Equipe de Geochimie de l'Environnement, LGIT, University of Grenoble and CNRS, B.P. 53, 38041 Grenoble, France
[2]Institut Laue-Langevin, B.P. 156, 38042 Grenoble, France
[3]Estacion Experimental del Zaidin, CSIC, C/ Profesor Abareda, 1, 18008 Granada, Spain
[4]Chemistry Department, University of Girona, Campus de Montilivi, 17071 Girona, Spain
[5]Department Applied Physics II, UPV/EHU and Ikerbasque, 48080 Bilbao, Spain
[6]European Synchrotron Radiation Facility, B.P. 220, 38043 Grenoble, France
[7]Institute of Environmental Assessment and Water Research, IDAEA, CSIC, Jordi Girona 18, 08034 Barcelona, Spain

Abstract

Schwertmannite is a poorly crystalline mineral that forms ochre rusts and precipitates in acid mine environments. Despite its ubiquity and its role as scavenger of important contaminants such as arsenic or selenium, its structure has not been yet determined. Here, a structure for schwertmannite is presented based on pair distribution function (PDF) data, X-ray diffraction (XRD) analyses, and density functional theory (DFT) calculations. We propose a structure formed by a deformed frame of iron octahedra similar to that of akaganeite. Simulations of X-ray diffraction patterns unveil the presence of long-range order associated with the position of the sulfate molecules, providing a useful way to discern two types of sulfate complexes in the structure. The simulations suggest that two sulfate molecules per unit cell are present in the structure forming one outer sphere and one inner sphere complex inside the channels formed by iron octahedra. Knowledge of the positions of the sulfates in the structure will help to better understand exchange processes with oxyanions of trace contaminants, such as arsenate, chromate, or selenate, that strongly influence their biogeochemical cycling in mining ecosystems.

Keywords: Schwertmannite, diffraction, structure, X-ray, pair distribution function, DFT, iron, sulfate

Introduction

Schwertmannite is a poorly crystalline ferric oxyhydroxysulfate that forms ochreous coatings on sulfide-bearing rocks and soils. It also precipitates in streams and lakes receiving acid-mine drainage where the weathering of iron sulfide minerals produces SO_4 and Fe^{2+} acid solutions. When exposed to the atmosphere, bacterially mediated oxidation of Fe^{2+} occurs and large quantities of nanoparticulate Fe^{3+} phases may form. Moreover, schwertmannite is a key solid in removing acidity in treatment systems where Fe^{2+} is rapidly oxidized by addition of alkalinity to acid mine drainage (Gagliano et al. 2004; Rotting et al. 2008). Further, in anoxic environments such as acid lakes, flooded soils, and wetlands, schwertmannite particles can serve as electron acceptor for Fe^{3+}-reducing bacteria, releasing the Fe^{2+} necessary for sulfate reduction and neoformation of iron sulfides (Burton et al. 2007). Schwertmannite forms aggregates of nanoparticles of typical hedgehog morphology.

Due to its high specific surface and positive charge in acid waters, schwertmannite efficiently removes oxyanions such as AsO_4^{3-}, SeO_4^{2-}, and CrO_4^{2-} from water (Carlson et al. 2002; Regenspurg and Peiffer 2005; Waychunas et al. 1995). However, despite its ubiquity and its important geochemical role, schwertmannite was only recently recognized as a mineral (Bigham

et al. 1994). Reasons for this late recognition include its poor crystallinity, its frequent association with more crystalline phases such as goethite and jarosite, and its metastable structure, which transforms into goethite and jarosite within months (Acero et al. 2006; Bigham et al. 1996).

The chemical composition of schwertmannite is also the object of controversy. Bigham et al. (1994) first proposed the chemical formula as $Fe_8O_8(OH)_{8-x}(SO_4)_x$, with x varying from 1 to 1.75. Yu et al. (1999) later estimated x to vary from 1.74 to 1.86. Uncertainty on the range of x values may be caused by the different location of the sulfate groups in the structure. The first approach to solve the structure of a "poorly crystalline sulfate oxyhydroxide" was reported by Bigham et al. (1990), who synthesized akaganeite-like materials with different concentrations of sulfate, that reproduced the 8-diffraction lines characteristic of schwertmannite, suggesting similarities between the octahedral framework of schwertmannite and akaganeite. Although some authors have proposed a ferrihydrite-like structure (Loan et al. 2004), there is more general agreement in the literature about this idea of the schwertmannite structure being akin to that of akaganeite, with a channel-like framework of FeO_6 octahedra (Barham 1997; Bigham et al. 1990; Waychunas et al. 2001, 1995). However, no clear experimental evidence on the structure or the positions of the sulfates has been reported yet. Recent publications by Figueiredo and da Silva (2007) and Majzlan and Myneni (2005) have suggested that pre-edge features in the X-ray

---

* E-mail: AFernandez-Martinez@lbl.gov

absorption near-edge structure (XANES) spectra at the S K-edge may be very useful in the study of sulfate speciation in schwertmannite. Majzlan and Myneni (2005) have linked the speciation of Fe^{3+} and SO_4^{2-} in solution to the speciation in schwertmannite, stating that H-bonding may be the main adsorption mechanism of sulfate at the schwertmannite-water interface. However, this attribution relies on data from Waychunas et al. (2001), where no XANES nor FTIR data are shown. In a recent paper, Boily et al. (2010) suggest from their analysis of their FTIR data that sulfate may form complexes both through hydrogen-bonding and direct binding to the iron structure. Figueiredo and da Silva (2007) have recently reported a collection of XANES spectra of different iron sulfate minerals, correlating the presence of a pre-edge shoulder with the number of O atoms shared between sulfate molecules and Fe octahedra. Future work, including schwertmannite XANES spectra, could shed more light on the exact sulfate speciation making use of the results by these two publications. Since trace element oxyanions like AsO_4^{3-}, SeO_4^{2-}, or CrO_4^{2-} replace SO_4^{2-}, knowing the allocation of the sulfate groups in the structure is essential to understand the retention of the oxyanions in the solid phase.

X-ray diffraction studies have been limited by the very small size of schwertmannite crystallites, which give broad diffraction peaks making it difficult to perform a detailed crystallographic analysis of the structure. In recent years, the pair distribution function (PDF) technique, classically known as the Patterson function technique (Guinier 1994), has been used to study poorly crystalline precipitates of environmental relevance like mackinawite (Michel et al. 2005; Scheinost et al. 2008), magnetite (Scheinost et al. 2008), or ferrihydrite (Michel et al. 2007a, 2007b). This technique relies on a Fourier transform of the whole diffraction pattern, and it is thus particularly well suited to the study of poorly crystalline phases of reduced crystallite size, where diffuse scattering has a significant contribution to the diffraction pattern. In this study, we present a combined high-energy X-ray diffraction and theoretical study of the structure of schwertmannite.

MATERIALS AND METHODS

Two types of schwertmannite specimens were used in this study: natural and synthetic. Natural samples were taken as fresh precipitates from the acid drainage in Monte Romero mine (Iberian Pyrite Belt), Spain. Synthetic schwertmannite was precipitated by adding ferric chloride to sodium sulfate solutions. The produced suspension was held at 60 °C for 12 min and then cooled to room temperature and dialysed for a period of 30 days (Schwertmann and Cornell 1991). Samples of natural schwertmannite were dried following two different procedures: air-dried and freeze-dried. This allowed us to check for any possible effect of the drying mechanism on the observed structure. Once dried, the powder samples were loaded into 0.8 mm diameter polymide capillaries that were sealed with wax.

High-energy X-ray total scattering experiments were performed at beamline ID15B of the European Synchrotron Radiation Facility, Grenoble, France. Scattering data were collected with a Pixium 4700 detector (Daniels and Drakopoulos 2009) using the rapid-acquisition pair distribution function technique (Chupas et al. 2003). Measurements of the samples, empty capillary, and the background were made at ambient temperature in a q-range of 0–25 $Å^{-1}$. The X-ray wavelength of 0.14252 Å was refined using a Ni standard. Corrections for sample-detector distance, tilt angle of the detector with respect to the direction of the incident radiation, and polarization were performed using Fit2D (Hammersley et al. 1995). Total scattering structure functions and pair distribution functions (PDF) were obtained using the PDFGetX2 software (Qiu et al. 2004). A crystalline standard (LaB_6) was measured and used to calculate the instrumental resolution effect on the PDF (Toby and Egami 1992). Fits of the PDFs were performed using the PDFGui software (Far-

row et al. 2007). In a PDF, the partial pair correlation functions between two atoms i and j, $g_{ij}(r)$, are weighted by a function, $w_{ij}(r)$ (Egami and Billinge 2003):

$$w_{ij} = c_i c_j \frac{f_i f_j}{\langle f \rangle^2} \tag{1}$$

c_i and c_j being the concentrations of the elements i and j, and f_i and f_j their atomic form factors evaluated at $q = 0$. q is the scattering vector

$$q = \frac{4\pi \sin(\theta)}{\lambda} \tag{2}$$

and

$$\langle f \rangle^2 = \left(\sum_i c_i f_i \right)^2 \tag{3}$$

The goodness of the refinements was checked using the weighted agreement factor R_w (Egami and Billinge 2003).

All the geometry optimizations were performed using the DFT code CASTEP (Clark et al. 2005). The calculations were performed using Vanderbilt ultrasoft pseudopotentials, with a plane-wave basis set energy cut-off of 760 eV and the Revised Perdew-Burke-Ernzerhof functional (Perdew et al. 1996) of the generalized gradient approximation (GGA). Brillouin zone integrations were done at special k-points determined according to the Monkhorst-Pack method, which gave six special k-points. Preliminary calculations were performed on akaganeite structure (Post et al. 2003) with the aim of tuning the convergence in k-points, pseudopotentials and energy cut-off. The obtained cell parameters show good agreement with the experimental values, within 1% (see Table 4).

Diffraction patterns of the resulting models of schwertmannite were generated using the code FORCITE (Accelrys Inc.). In this code, the diffraction pattern is calculated using the Debye formula of diffraction

$$I_N(q) = \sum_{n,m \neq n}^{N} f_n(q) f_m(q) \frac{\sin(qr_{nm})}{qr_{nm}} \tag{4}$$

where r_{nm} is the distance between two pair of atoms n and m. A cutoff of 40 Å was used, meaning that only pairs of atoms placed at a distance $r_{nm} < 40$ Å were included in the calculation.

The structure of akaganeite is composed of double chains of iron (95% occupancy) or nickel (5% occupancy) oxide (or hydroxide) octahedra, which share corners to form square 2×2 tunnels (see Fig. 2) (Post et al. 2003). Each unit cell has two identical tunnels, with centers at (0, 0, 0) and (0.5, 0.5, 0.5) of the akaganeite unit cell. A note has to be made here about the indexing of the akaganeite and schwertmannite structures. In the early studies of schwertmannite by Bigham et al. (1990), the authors used an indexation in which the the channel of akaganeite's structure lies parallel to the c axis. However, we built our models from the akaganeite structure published by Post et al. (2003) in which the channel extends along the b axis of akaganeite's unit cell. We will use the setting of Post et al. (2003) in the text, with the exception that we have interchanged the a and b axis and reversed the sign of c to keep a right-handed coordinate system with an obtuse β angle.

The research strategy followed in this work is as follows: the structure of akaganeite was modified replacing all the nickel atoms by iron atoms. A supercell $1 \times 2 \times 1$ was created, and the chlorine atoms were substituted by two sulfate molecules forming bidentate inner-sphere complexes on the internal surface of akaganeite's channel (we call this model "sulfate-doped akaganeite"). Charge imbalance originated by these substitutions can be equilibrated by the deprotonation of doubly protonated hydroxyl groups existing in the structure of akaganeite. The PDF of the sulfate-doped akaganeite structure was simulated to determine the sensitivity of the X-ray PDF technique with respect to the relative positions of the different atoms within the unit cell. As it can be seen it Figure 1, the result of the simulation shows that the PDF technique is mostly sensitive to the relative positions of Fe and O atoms only. The contribution of the sulfate molecules to the total PDF is very low, as it could be expected from previous theoretical estimations done using Equations 1–3. The atomic form factor f_i is proportional to the atomic number Z. Of all the elements present in the structure of schwertmannite, iron is the one with highest atomic number ($Z_{Fe} = 26$), which emphasizes the weighting factors of the atomic pair-correlations (Eq. 1) involving iron atoms. This structure was used as the initial model for the fitting of the PDF data, imposing only translational $P1$ symmetry. In a first fit, the x and z coordinates of the iron atoms, the lattice parameters a, b, c, and β, the isotropic thermal atomic displacement parameters U, the particle size d, and the peak broadening factor σ_q were refined. In a second run, once the fits

were close to local minima, the x and z atomic coordinates of the oxygen atom were also refined. Care was taken that the results fulfilled basic crystal-chemistry rules, including minimum distances for Fe-O of 1.75 Å. The reason why only the x and z atomic coordinates were refined is because we expect the changes in the structure coming from changes in the a and c lattice parameters, or from changes in the value of the β angle. The reason for not refining the positions of the sulfur and O atoms from the sulfate molecules is that, as shown in Figure 1 and stated above, the correlations between Fe-Fe and Fe-O atom pairs are the dominant contributions in the PDF of schwertmannite. A recent publication and the results presented in this article suggest the existence of inner-sphere sulfate complexes in the structure of schwertmannite (Boily et al. 2010). Simple bond valence considerations suggest that a high degree of distortions may be present in the geometry of the iron octahedra to allow surface O atoms shared with sulfate molecules to satisfy bond valence requirements. For this reason, Fe-O bond lengths as short as 1.75 Å have been allowed to occur.

In parallel, the sulfate-doped akaganeite was optimized using DFT to understand some trends observed in the structures obtained in the PDF refinements. Charge equilibration was ensured in the unit cells by adjusting the number of hydrogen atoms present in the structures as OH groups so the total charge is zero. In addition, powder diffraction patterns were simulated and compared to alternative structures to check the consistency between the short-range order revealed by PDF analyses and the long-range order underlying the diffraction patterns.

PDF-fitted structures of the octahedral framework of schwertmannite are provided in accompanying CIF files[1].

---

[1] Deposit item AM-10-041, CIF. Deposit items are available two ways: For a paper copy contact the Business Office of the Mineralogical Society of America (see inside front cover of recent issue) for price information. For an electronic copy visit the MSA web site at http://www.minsocam.org, go to the *American Mineralogist* Contents, find the table of contents for the specific volume/issue wanted, and then click on the deposit link there.
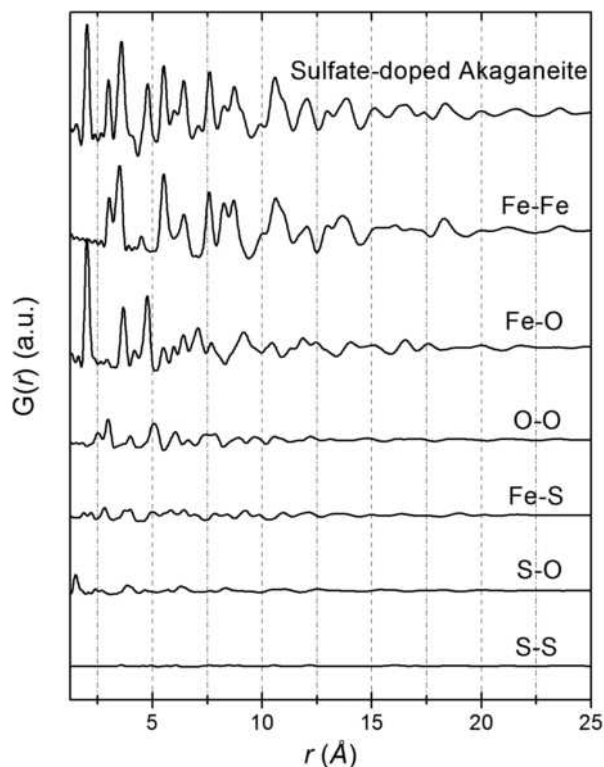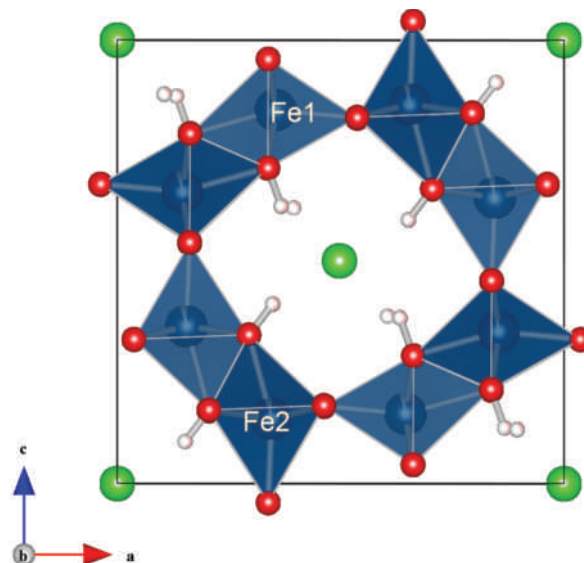

FIGURE 2. Structure of akaganeite. The octahedra are formed by iron (95%) or nickel (5%) atoms (blue) surrounded by six O atoms (red). The tunnel structure is occupied by chlorine atoms (green). The distance between atoms Fe1 and Fe2 is equal to d = 7.5 Å, and can be clearly distinguished in the PDF of akaganeite (Fig. 3). Color online.

RESULTS AND DISCUSSION

Octahedral framework

PDFs of the natural and synthetic schwertmannite samples and simulated PDFs of the akaganeite (Post et al. 2003) and sulfate-doped akaganeite before and after DFT-optimization are presented in Figure 3. PDF-fitted structures of the octahedral framework of schwertmannite are given in Table 1; atomic coordinates are given in Tables 2 and 3. No major differences can be found between the PDFs of air-dried and freeze-dried samples. This indicates that, in contrast to ferrihydrite (Greffie et al. 2001), the schwertmannite structure does not undergo any major structural modifications when freeze-dried. The main difference is a slight increase in the intensity of the first peak in the PDF of natural freeze-dried schwertmannite. However, we do not think this is a structural effect nor a consequence of the drying procedure, as (1) the intensity of this peak is affected by vibrational correlations (Egami and Billinge 2003), and (2) we do not observe the same effect in the freeze-dried synthetic schwertmannite. A comparison with the PDF of the crystalline standard LaB_6 (not shown) allows estimating the size of the coherent domains of schwertmannite. The decay in the intensity of the PDF of LaB_6 at high r values can be ascribed to the effect of instrumental resolution (Toby and Egami 1992). Instead, a more pronounced decay (within the instrumental resolution) is found in the PDF of the schwertmannite samples. Fits of this decay with a function reproducing particles of spherical shape (Gilbert 2008) yield an average particle diameter of 3–4 nm (see Table 1). The small size of the coherent domains contrasts with that of schwertmannite aggregates, which are usually described as having hedgehog-like morphologies with needles in the range of the micrometer.

FIGURE 1. Simulated PDF of sulfate-doped akaganeite with its partial PDFs. The partial PDFs are weighted by their weighting functions, w_{ij}.

TABLE 1. Results of the PDF refinements

	Natural freeze-dried, $P1$	Natural air-dried, $P1$	Synthetic freeze-dried, $P1$	LaB$_6$, $Pm\bar{3}m$
a (Å)	10.752(8)	10.821(1)	10.862(4)	4.1594(4)
b (Å)	6.036(2)	6.002(2)	6.031(4)	
c (Å)	10.497(6)	10.514(8)	10.471(7)	
β (°)	93.3(5)	92.6(7)	92.5(3)	
V (Å^3)	680.1(3)	682.2(3)	685.3(4)	71.960(1)
U_{Fe} (Å^2)	0.002(2)	0.002(1)	0.003(2)	
U_O (Å^2)	0.009(1)	0.009(5)	0.009(6)	
U_S (Å^2)*	0.015	0.015	0.015	
U_{La} (Å^2)				0.0044(4)
U_B (Å^2)				0.0107(2)
d (Å)	30.9(1)	31.11(4)	40.7(3)	∞
σ_q (Å^{-1})†	0.0309	0.0309	0.0309	0.0309(1)
R_w (%)	26.70	24.50	23.04	17.85

Notes: U stands for the isotropic thermal displacement contributing to the Debye-Waller factor, σ_q is the instrumental dampening factor of the PDFs originated by the limited *q*-resolution, *d* is the diameter of the coherent domain size (spherical approximation), and R_w is the weighted agreement factor.
* U_S was fixed to an estimated value of $U_S = 0.015$ Å^2.
† The value of the dampening factor was calculated for the LaB$_6$ standard and kept constant during the refinements of the schwertmannite PDFs.

TABLE 2. Atomic coordinates of Model 1

Atom	x	y	z
Fe	0.345(5)	0	0.152(3)
Fe	0.140(5)	0	0.645(4)
O	0.288(8)	0	0.322(7)
O	0.043(8)	0	0.336(9)
O	0.335(9)	0	0.690(1)
O	0.325(6)	0	0.946(5)
Fe	0.857(7)	0.25	0.611(6)
Fe	0.700(4)	0.25	0.093(5)
O	0.787(5)	0.25	0.796(7)
O	0.540(1)	0.25	0.810(4)
O	0.861(6)	0.25	0.159(7)
O	0.824(6)	0.25	0.419(7)
Fe	0.669(5)	0	0.811(4)
Fe	0.866(4)	0	0.320(3)
O	0.711(5)	0	0.626(6)
O	0.956(6)	0	0.612(8)
O	0.664(5)	0	0.260(7)
O	0.674(7)	0	0.002(8)
Fe	0.151(4)	0.25	0.352(4)
Fe	0.344(3)	0.25	0.840(5)
O	0.211(6)	0.25	0.152(7)
O	0.456(7)	0.25	0.138(7)
O	0.165(6)	0.25	0.786(7)
O	0.175(7)	0.25	0.527(8)
Fe	0.337(5)	0.5	0.142(4)
Fe	0.144(4)	0.5	0.648(5)
O	0.288(5)	0.5	0.322(5)
O	0.043(7)	0.5	0.336(7)
O	0.335(8)	0.5	0.690(1)
O	0.325(3)	0.5	0.946(5)
Fe	0.846(3)	0.75	0.606(4)
Fe	0.696(4)	0.75	0.095(3)
O	0.787(6)	0.75	0.796(8)
O	0.542(7)	0.75	0.810(6)
O	0.857(1)	0.75	0.157(1)
O	0.824(7)	0.75	0.419(7)
Fe	0.666(4)	0.5	0.804(3)
Fe	0.865(5)	0.5	0.322(3)
O	0.711(6)	0.5	0.626(8)
O	0.956(7)	0.5	0.612(7)
O	0.664(6)	0.5	0.260(6)
O	0.674(6)	0.5	0.002(7)
Fe	0.153(5)	0.75	0.338(5)
Fe	0.363(4)	0.75	0.835(5)
O	0.211(6)	0.75	0.150(1)
O	0.456(6)	0.75	0.138(6)
O	0.165(7)	0.75	0.786(6)
O	0.175(6)	0.75	0.528(7)

TABLE 3. Atomic coordinates of Model 2

Atom	x	y	z
Fe	0.345(1)	0	0.122(3)
Fe	0.150(6)	0	0.626(9)
O	0.288(3)	0	0.307(4)
O	0.052(1)	0	0.334(5)
O	0.334(5)	0	0.67(1)
O	0.324(1)	0	0.929(3)
Fe	0.883(7)	0.25	0.560(2)
Fe	0.710(2)	0.25	0.054(9)
O	0.786(2)	0.25	0.756(2)
O	0.541(5)	0.25	0.782(4)
O	0.866(6)	0.25	0.126(3)
O	0.822(3)	0.25	0.378(1)
Fe	0.688(6)	0	0.770(1)
Fe	0.897(3)	0	0.266(5)
O	0.709(7)	0	0.590(1)
O	0.964(8)	0	0.563(9)
O	0.690(2)	0	0.208(5)
O	0.691(2)	0	0.959(9)
Fe	0.158(7)	0.25	0.323(8)
Fe	0.338(4)	0.25	0.835(8)
O	0.211(2)	0.25	0.141(3)
O	0.455(7)	0.25	0.115(1)
O	0.164(2)	0.25	0.777(7)
O	0.174(6)	0.25	0.519(4)
Fe	0.328(5)	0.5	0.117(1)
Fe	0.155(9)	0.5	0.624(1)
O	0.287(6)	0.5	0.307(4)
O	0.042(6)	0.5	0.333(6)
O	0.335(5)	0.5	0.671(3)
O	0.324(2)	0.5	0.929(3)
Fe	0.841(3)	0.75	0.554(3)
Fe	0.845(1)	0.75	0.956(6)
O	0.786(1)	0.75	0.765(7)
O	0.541(5)	0.75	0.782(4)
O	0.854(2)	0.75	0.138(2)
O	0.822(6)	0.75	0.378(1)
Fe	0.668(5)	0.5	0.771(1)
Fe	0.867(8)	0.5	0.271(7)
O	0.709(8)	0.5	0.590(1)
O	0.964(6)	0.5	0.563(6)
O	0.691(5)	0.5	0.959(9)
Fe	0.147(4)	0.75	0.322(1)
Fe	0.353(3)	0.75	0.821(1)
O	0.211(4)	0.75	0.141(3)
O	0.455(2)	0.75	0.115(1)
O	0.164(1)	0.75	0.777(7)
O	0.174(7)	0.75	0.519(4)
O	0.969(5)	0.5	0.958(5)
O	0.969(8)	0	0.958(5)
O	0.690(6)	0.5	0.213(6)

identified in the region from 1 to 7 Å: the position of the first peak at ~1.98 Å is the same for both structures. It corresponds to the Fe-O distance of Fe^{3+} in octahedral coordination. The presence of sulfates in sulfate-doped akaganeite and in schwertmannite can be discerned from a small peak appearing at a distance of ~1.64 Å, which corresponds to the S-O distance. The peaks at ~3 and ~3.45 Å, better resolved in the modeled PDFs of akaganeite, correspond to Fe-Fe distances of different types of edge-sharing iron octahedra: the distance at ~3 Å corresponds to two iron octahedra lying on the same equatorial plane, while the distance at ~3.45 Å comes from edge-sharing iron octahedra with different equatorial planes. The next three peaks (4.75, 5.45, and 6.33 Å) correspond to Fe-Fe and Fe-O correlations. Although there are some small differences, their positions and intensities are very similar. The main differences between these two structures arise from correlations in the region 7 Å $< r <$ 10 Å. A significant decrease in the intensity of the peak at $r = 7.5$ Å is observed in the PDF of the schwertmannite samples. This

The PDFs of akaganeite and schwertmannite structures reveal very similar local structures. Common structural features can be

peak corresponds to correlations between iron atoms placed on opposite sides of the akaganeite's channel (atoms Fe1 and Fe2 in Fig. 2). However, its intensity is affected by the presence of sulfate molecules in the structure, as can be observed in the case of sulfate-doped akaganeite, where it has lower intensity.

Fitting of the PDF data were performed with the aim of explaining the differences observed between the theoretical PDFs of akaganeite and sulfate-doped akaganeite, and the experimental PDFs of schwertmannite. The structure of sulfate-doped akaganeite was used as initial model in the refinements. The results of the refinements are presented in Figure 4. All the fits converged yielding a structure where the initial akaganeite unit cell was deformed, with values of the β angle around $\beta \approx 93°$ (Table 1). This deformation was observed in all the fits performed. We found a monoclinic unit cell, with three different values for the parameters a, b, and c (see lattice parameters in Table 1). The unit-cell parameters obtained differ from those proposed by Bigham et al. (1994), who proposed a tetragonal unit cell with lattice parameters $a = c = 10.66$ Å and $b = 6.04$ Å.

The different values found for the lattice parameters a and c provide a partial explanation for the decreasing of the intensity of the correlation at $r = 7.5$ Å. A splitting of this distance into several distances in the range between 7.4–7.8 Å is found in the refined structures. This splitting is reflected in the PDF of schwertmannite by a decrease in the peak intensity and a broadening of its width. As shown in Figure 3, the presence of
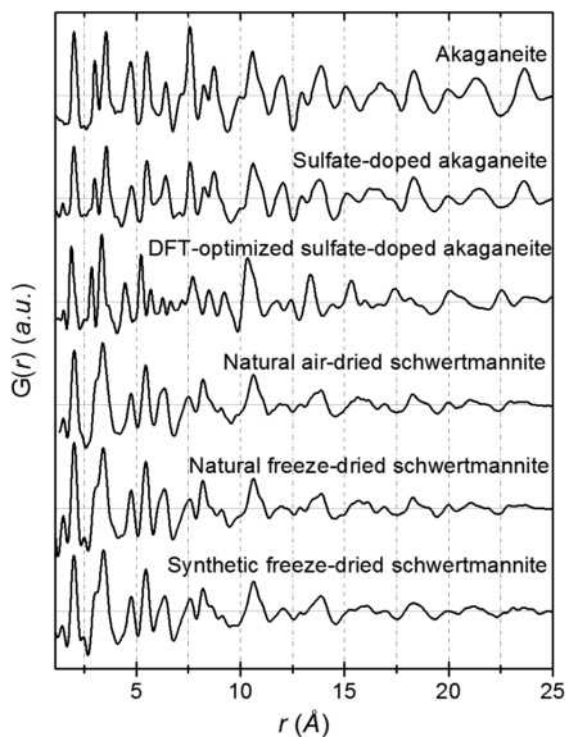

FIGURE 3. Simulated PDFs of akaganeite and of sulfate-doped akaganeite before and after DFT optimization, and experimental PDFs of schwertmannite samples. The decay in the intensity seen at high r in the schwertmannite PDFs has been taken into account in the simulated PDFs by using the instrumental dampening factor obtained from the refinement of the LaB$_6$.

TABLE 4. Unit-cell parameters and volume of the optimized and experimental akaganeite structures (Post et al. 2003) and of the optimized sulfate-doped akaganeite structure

Structure	a (Å)	b (Å)	c (Å)	α (°)	β (°)	γ (°)	V (Å³)
DFT-optimized akaganeite	10.45	3.07	10.45	90.00	89.75	89.91	337
Experimental akaganeite	10.5876(5)	3.03357(8)	10.5277(6)	90	90.14(2)*	90	338.13(2)
DFT-optimized sulfate-doped akaganeite	10.55	6.03†	10.59	90.47	92.61	89.40	674

* Note that our coordinate system differs from that of Post et al. (2003) in that we have interchanged the a and c axis to keep a right-handed system with an obtuse β angle.
† The structure of sulfate-doped akaganeite was formed from a supercell 1 × 2 × 1 of akaganeite. This is the reason why the b parameter and the volume are almost double than for akaganeite.

sulfates in the structure affects the intensity of this peak, too. Two different configurations for the iron atoms within the unit cell of schwertmannite resulted from the PDF refinements. In a first model (Model 1), the distortion of the β angle causes the distance between some adjacent iron atoms (Fe1 and Fe2 in Fig. 5) to become too long to form two corner-sharing iron octahedra ($d \sim 4.3$ Å). This model was obtained after the fitting procedure of the PDF of the natural freeze-dried schwertmannite sample. In the second model (Model 2), the distance between adjacent Fe octahedra (Fe2 and Fe3 in Fig. 6) is also too long ($d \sim 4.33$ Å) and the Fe1 octahedron is rotated by 90°, sharing an edge with an iron octahedron from the neighbor frame (Fig. 6). This second structure resulted from the fitting of the natural air-dried and synthetic freeze-dried schwertmannite samples. The fact that the PDFs of the three samples are almost identical and that the agreement factors of the three fits lie in the same range (Table 1) tells us about the non-uniqueness of the result. The two models thus cannot be distinguished within the experimental resolution of the data. As shown in Table 1, the obtained lattice parameters have large errors (in the order of 10^{-2} to 10^{-3} Å) in comparison to the values obtained for the crystalline standard ($\sim 10^{-4}$ Å). There are two reasons for this: (1) the coherent domain size of schwertmannite is about ~ 3 nm. This implies that a coherent domain would be formed, on average, by a 3 × 5 × 3 supercell. It seems then plausible that such a small particle is affected by structural relaxations at the surface, causing that the lattice parameters of the unit cells close to the surface have large deviations from those of the unit cells in the "bulk" of the nanoparticle. (2) Our approach is limited because we have chosen to use a periodic system with a relatively small unit cell (in comparison with the size of the nanoparticle) to describe the structure of a disordered nanoparticle.

To better understand the origin of the deformation of the unit cell, we performed DFT-based geometry optimization of the structure of sulfate-doped akaganeite. This structure has two sulfate molecules forming bidentate inner-sphere complexes (C_{2v} symmetry). The optimized and non-optimized structures are shown in Figure 7, and their cell parameters are given in Table 4. The simulated PDF of the DFT-optimized model of sulfate-doped akaganeite (Fig. 3) compares very well with the PDFs from schwertmannite, although most of the peaks are displaced towards lower distances. This may be caused by an underestimation of the Fe-O distance, with its peak position

decreasing from $r = 2.01$ Å in the experimental PDFs to $r = 1.88$ Å in the DFT-optimized structure. As it can be seen in Figure 7, the optimized structure has a rectangular channel causing a decrease in the intensity of the peak at $r = 7.5$ Å, and the appearance of two small peaks corresponding to iron atoms placed at adjacent sides of the channel are found at $r < 7.5$ Å. This small deformation of the channel can be caused by the lack of water molecules in the optimized structure and by the uncertainty in the positions of the hydroxyl surface groups. Water molecules and surface hydroxyls are expected to play an important role in the structure of schwertmannite, since they will form a network of hydrogen bonding interactions that may cause the structure to swell. However, the initial positions of water and hydroxyl groups in the DFT optimization procedure are a critical parameter in the optimization procedure, strongly influencing the geometry of the final optimized structure. Unfortunately, the inclusion of water molecules entails a high increase in the degrees of freedom of the system, and thus we have preferred not to consider this interaction in our simulated structures. In spite of this, a structure deformed in a similar way as the experimentally observed one with $\beta \approx 93°$ was obtained. The volume of the optimized cell ($V = 675$ Å³) is slightly smaller than the experimental value for schwertmannite reported by Bigham et al. (1994) ($V = 687$ Å³), and it is in the same order of magnitude of the experimental values found by our PDF analysis (see Table 1). The deformation

of the unit cell can be monitored by looking at the values of the stress tensor calculated by CASTEP after the first optimization step. The presence of the sulfate molecules in the structure makes that the off-diagonal elements σ_{xz} and σ_{zx} have values higher than zero, indicating a shear stress that leads to the deformation of the angle β of the unit cell (see Table 5). The non-zero values of the

FIGURE 5. The $2 \times 1 \times 2$ supercell of the Model 1 obtained after PDF fitting. Only the positions of the iron atoms were refined. The distance from Fe1 to Fe2 is too long to form two corner-sharing octahedra (illustrated with dotted line). Color online.
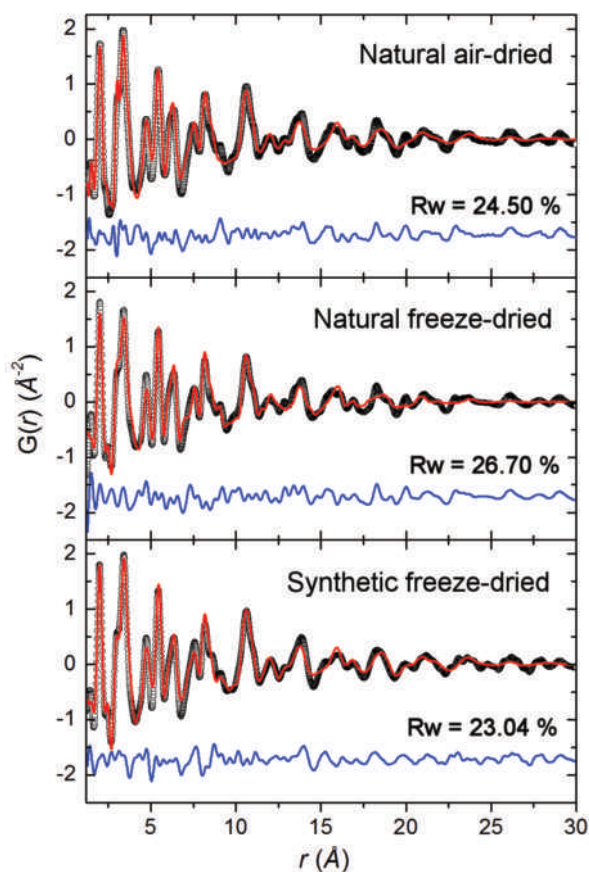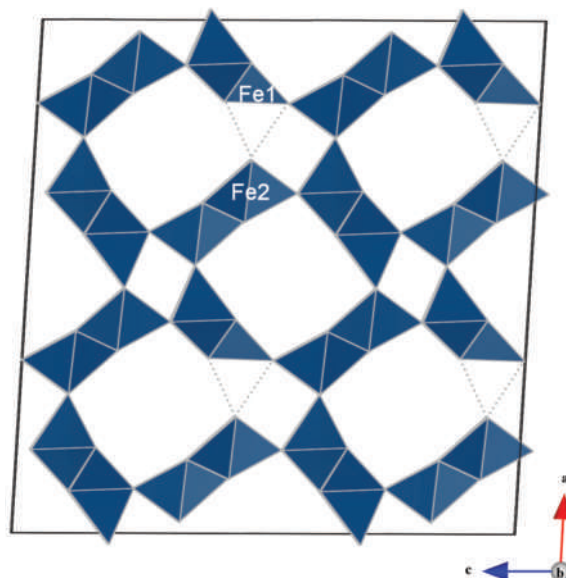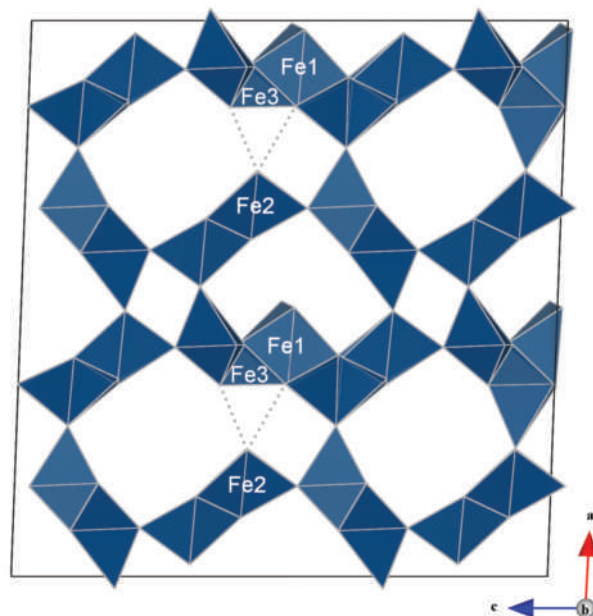

FIGURE 4. Experimental PDF data (black circles) fitted by the refined model PDF (red line). A difference plot (blue line) is included beneath each data set. Color online.

FIGURE 6. $2 \times 1 \times 2$ supercell of the Model 2 obtained after PDF fitting. Only the positions of the iron atoms were refined. One Fe1 octahedron is turned by 90°, sharing two edges with two neighboring iron atoms, and a second one (Fe3, displaced along the b axis with respect to Fe1) is too far from its neighbor (Fe2) to form a corner-sharing configuration. Color online.

diagonal elements (σ_{xx}, σ_{yy}, and σ_{zz}) are responsible for changes in the lattice parameters and thus do not induce deformations of the unit-cell angles. The fact that this deformed structure fits the experimental PDF data well supports thus the hypothesis, suggested by FTIR data (Jonsson et al. 2005; Peak et al. 1999), that these inner-sphere complexes, with sulfates having C_{2v} symmetry, actually exist in the schwertmannite structure. It is worth noting the existence of a similar deformation in the unit cell of nanometric akaganeite (Deore et al. 2005). These authors have evoked surface energy as the driving parameter for the transition from a tetragonal to a monoclinic phase when the size of the akaganeite particles is decreased. Although a value for the coherent domain size has been estimated for schwertmannite from the PDF measurements, with a value between 3–4 nm, the concept of "particle surface" is not of straightforward application in this case. Our proposed structure for the schwertmannite octahedral framework is composed of a highly defective entangled network of structural motifs like those presented in Models 1 and 2. The existence of these defects can produce strains in the structure, reducing the coherent domain size to values smaller than the actual particle size. We consider that these effects (structural strains induced by the presence of defects) or the presence of inner-sphere bidentate sulfate complexes (as shown here by DFT calculations) may be the main driving force for the deformation of the structure, apart from surface energetics, as proposed by Deore et al. (2005) for akaganeite.

Position of the sulfate molecules

The non-overlapping first two peaks in the schwertmannite PDFs, corresponding to S-O and Fe-O atomic correlations, and Equation 1 provide an indirect way to estimate the concentration of sulfates in the samples. According to Equation 1, the weighting factors of each correlation can be expressed as

$$\text{S-O correlation: } w_{\text{S-O}} = c_{\text{S}}c_{\text{O1}}\frac{Z_{\text{S}}Z_{\text{O}}}{\langle f \rangle^2} = 4c_{\text{S}}^2\frac{Z_{\text{S}}Z_{\text{O}}}{\langle f \rangle^2} \tag{5}$$

$$\text{Fe-O correlation: } w_{\text{Fe-O}} = c_{\text{Fe}}c_{\text{O2}}\frac{Z_{\text{Fe}}Z_{\text{O}}}{\langle f \rangle^2} \tag{6}$$

where c_{S} and c_{Fe} are the concentrations of sulfur and iron atoms respectively, c_{O1} is the concentration of O atoms from sulfate molecules, which has been fixed to $c_{\text{O1}} = 4c_{\text{S}}$, c_{O2} is the concentration of O atoms from iron octahedra, Z_{Fe} and Z_{S} are respectively the atomic numbers of iron and sulfur. In the PDF, the ratio of intensities of both correlations is proportional to the ration between the weighting factors, yielding

$$c_{\text{S}} = \sqrt{\frac{I_{\text{S-O}}}{I_{\text{Fe-O}}}\frac{Z_{\text{Fe}}}{Z_{\text{S}}}\frac{c_{\text{Fe}}c_{\text{O2}}}{4}} \tag{7}$$

where $I_{\text{S-O}}$ and $I_{\text{Fe-O}}$ are the intensities of the peaks corresponding to the S-O and Fe-O correlations measured from the baseline of the PDF. Application of this formula to the PDFs of the three schwertmannite samples yields an average value of $c_{\text{S}} = 0.1 \pm 0.03$, which corresponds to a sulfate content in the schwertmannite unit cell used in this work (containing 16 Fe atoms) of 6.4

TABLE 5. Stress tensor calculated after the first step of the DFT-geometry optimization of the sulfate-doped akaganeite structure

σ_{ij} (GPa)	x	y	z
x	9.88	−0.02	−2.44
y	−0.02	1.30	−0.19
z	−2.44	−0.19	−2.68

Note: The off-diagonal elements σ_{xz} and σ_{zx} indicate a shear stress responsible of the deformation of the angle β.
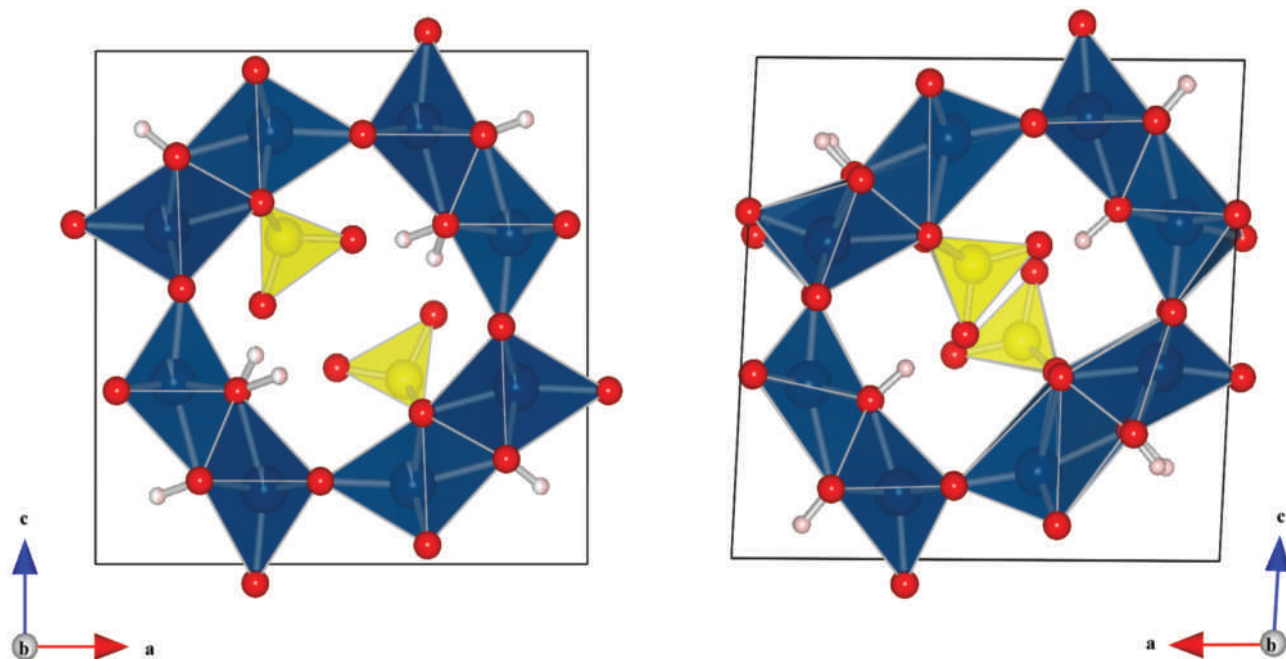

FIGURE 7. Structure of sulfate-doped akaganeite before (**left**) and after (**right**) being optimized using DFT-based calculations. Note the change in the coordinate-system to keep β > 90°. Color online.

± 2 sulfate molecules per unit cell. The high uncertainty in this value comes from the fact that the first peaks in the PDF, notably the peak corresponding to the S-O correlation, are affected by the Fourier oscillations originated by the Fourier transform of the intensity data. In addition, the baseline is poorly defined in this region of the PDF making a precise measurement of the peak intensity more difficult. The resulting sulfate concentration is higher than the reported concentrations calculated by analytical chemistry methods, which range from 2 to 3.72 sulfate molecules per unit cell (Bigham et al. 1990; Yu et al. 1999).

It is important to note that the PDF of schwertmannite is dominated by correlations involving iron and O atoms (see Fig. 1). This implies that only the short-range order of the octahedral framework is refined in the PDF fitting procedure, rendering the determination of (1) the exact positions of the sulfates within the cell and (2) their orientations within the unit cell of schwertmannite from PDF data analysis impossible. In addition, PDF analysis gives information only about the local or short-range order of the schwertmannite structure. Information about the long-range order can be extracted by analyzing the powder diffraction pattern. This kind of analysis has been hindered by the broad diffraction peaks found in the schwertmannite diffraction patterns. For this reason, the use of X-ray diffraction for structural studies has been limited in the schwertmannite literature, serving mainly as a fingerprint for identification purposes. In contrast to these data collected by laboratory X-ray sources, synchrotron powder-diffraction data have a higher resolution and allow us to use it as a reference to compare our modeled powder diffraction patterns.

The fitting range used in our PDF analyses extended from 1 to 30 Å, which is longer than the three lattice parameters of the structural models used as input in the analyses. This implies that the long-range order arising from repetitions along the unit cell axes is already taken into account in the PDF analysis, and thus the resulting structure should reproduce both short-range and long-range order along the three dimensional directions. To check this consistency, we have calculated theoretical powder diffraction patterns of the refined structures, varying the number and positions of the sulfates molecules within the unit cell. The calculated diffraction patterns of schwertmannite Models 1 and 2 are presented in Figure 8 and compared to the experimental patterns. It is important to note that, due to the different a and c lattice parameters, single peaks of akaganeite are split into two or more different peaks in schwertmannite diffraction patterns. However, due to the small coherent domain sizes of schwertmannite, these split reflections overlap, making it impossible to accurately determine their positions and intensities. This high degree of overlapping has prevented the application of analysis techniques such as Le Bail or Rietveld fits, which would be very useful to precisely determine the cell parameters. From now on, we will continue to use the original notation of akaganeite when referring to the diffraction lines, even though some of them are composed by several overlapping reflections due to the small size of the coherent domains. Note that in the accompanying CIF files[1] the axis a and c have been interchanged and a has been changed to $-a$ to keep a righ-handed coordinate system with $\beta > 90°$. There are only small differences between the two models, the most significant being a higher intensity for the (042) and (524) reflections of Model 2, which agrees better

with the experimentally observed. The calculated patterns are in quite good agreement with the experimental ones, except for the intensities of some lines. The (040) reflection is lower in the Model 1 and 2 patterns than in the experiments and the (200) and (101) reflections have higher intensity in the models. This is especially true for the (101) reflection, which is absent in the experimental patterns. Bigham et al. (1990) observed how the intensity of this reflection decreased proportionally to the amount of sulfate added during the precipitation of akaganeite. They found that schwertmannite was the only precipitation product formed when the synthesis was made in the presence of 2000 ppm of sulfate. The precipitate showed the typical 8 diffraction lines characteristic of schwertmannite, while the akaganeite (101) reflection was missing. We have checked this correlation between the intensity of the (101) line and the unit-cell sulfate content by generating a series of diffraction patterns of the schwertmannite structure obtained from the PDF analysis loaded with different amounts of sulfate molecules. Only two different kind of sulfate molecules were considered: (1) a bidentate inner-sphere complex placed sharing two O atoms with the iron framework, as shown in Figure 9a (the shared O atoms were chosen to have the same x and z coordinates, but placed at a different y coordinate), and (2) an outer-sphere complex placed in the center of the channel, as shown in Figure 9a. All the calculations were performed using the structure of Model 1 for the octahedral framework. The results are presented in Figure 9b. Only the intensities of the reflections (101), (200), (301), (023), (042), and (524) are sensitive to the concentration of sulfate molecules in the structure and to their positions within the unit cell. The most important variations of intensity are found for the diffraction peaks (101), (200), and (301), as shown in Figures 9c–9e. The intensity of the (101) peak decreases as long as more sulfates are introduced in the channel of the octahedral framework of schwertmannite, as reported by Bigham et al. (1990). The best agreement with the experimental intensity, with the (101) reflection practically absent, is found when four sulfates form outer-sphere complexes are present in the structure. The evolution of the (200) and (301) intensity shows opposite behaviors. The intensity of these two peaks are dependent on the positions of the sulfate within the structure. Their relative peak intensities have been calculated using the intensity of line (221) (the more intense in the experimental patterns) and are presented in Table 6. A maximum intensity for the (200) reflection is found when four inner-sphere complexes are present in the structure. On the other hand, a maximum is found for the (301) peak for the structure with four outer-sphere complexes. The relative intensities of these two peaks can thus be used to estimate the sulfate content and the binding mechanisms to the structure, by comparison to the experimental values (see Table 6). Simulations of structures where sulfates are present both as inner- and outer-sphere complexes were then performed to better reproduce the experimental data. The results are presented in Figure 10, and compared with the experimental data. Relative intensities are reported in Table 6. If only sulfates are considered to be present, none of the combinations matched the relative intensities found in the experimental patterns [see for example the intensity ratios of the structure with 4 outer-sphere SO_4 complexes in Table 6, which yield good $I_{(101)}/I_{(221)}$ and $I_{(200)}/I_{(221)}$ but very bad agreement for the $I_{(301)}/I_{(221)}$]. For this reason, we
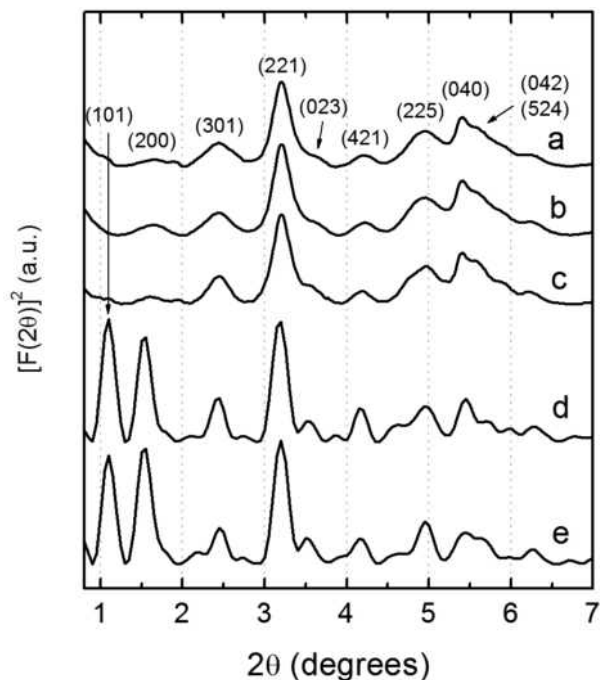
FIGURE 8. Diffraction patterns of (**a**) natural air-dried schwertmannite; (**b**) natural freeze-dried schwertmannite; (**c**) synthetic freeze-dried schwertmannite; (**d**) Model 1; and (**e**) Model 2.

have considered the case where water is present in the structure. This hypothesis is supported by thermo-gravimetric data of Yu et al. (1999), who reported a range of 8.5 to 8.9 water molecules per unit cell, and it seems to be very reasonable in view of the exchange processes taking place between sulfates and other oxyanions, which are hydrated species. Preliminary calculations including eight molecules per cell do improve the agreement with the experimental XRD pattern (see Fig. 10). The determination of the exact positions of the water molecules within the unit cell is challenging, especially using X-ray radiation as experimental probe. The use of DFT calculations is also limited by the fact that there are many degrees of freedom in the system, and it becomes thus difficult to explore all the possibilities of the positions of water molecules and outer-sphere sulfate molecules. For these reasons, the water molecules were placed in the structure with the only care that the minimum distance between atoms from different water molecules was 1.8 Å, as expected from hydrogen bonded water molecules. The best agreement with the experiment, as reported in Table 6, is found for the structure containing two outer-sphere and two inner-sphere complexes with 8 water molecules per unit cell. This explains the range of stoichiometry reported for the mineral formula, with SO_4 varying from 2 to 3.72 for each 16 Fe atoms (Bigham et al. 1994; Yu et al. 1999). The lower limit is coincident with the number of inner-sphere complexes in the structure, whereas the rest corresponds to outer-sphere complexes. This result suggests that the variability in the
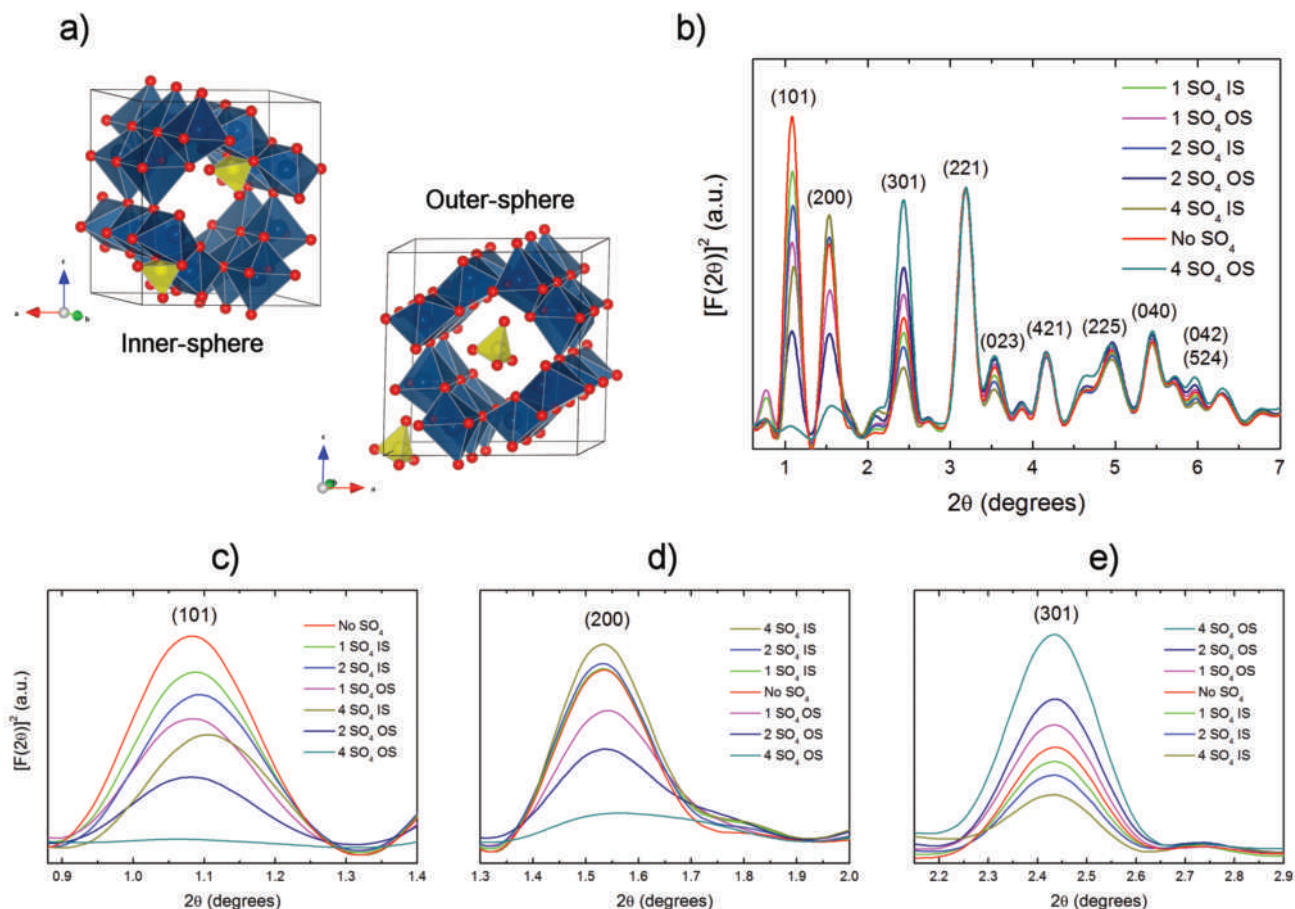

FIGURE 9. Diffraction patterns of Model 1, loaded with different amounts of sulfate molecules. Color online.

TABLE 6. Values of the relative intensity of the (101), (200), and (301) reflections for different structures with inner-sphere (IS) and outer-sphere (OS) sulfate complexes

Structure	$I_{(101)}/I_{(221)}$	$I_{(200)}/I_{(221)}$	$I_{(301)}/I_{(221)}$
No SO_4	1.28	0.78	0.48
1 SO_4IS	1.06	0.79	0.42
2 SO_4IS	0.93	0.81	0.37
1 SO_4OS	0.78	0.59	0.57
4 SO_4IS	0.69	0.88	0.28
2 SO_4OS	0.43	0.42	0.68
4 SO_4OS	0.05	0.13	0.95
Natural air-dried schwertmannite	**0.04**	**0.08**	**0.28**
2 SO_4IS + 2 SO_4OS	0.29	0.38	0.52
4 SO_4IS + 2 SO_4OS	0.20	0.48	0.41
2 SO_4IS + 2 SO_4OS + 8 H_2O	**0.11**	**0.26**	**0.47**

Notes: The intensity of the (221) reflection is used as reference. The best agreement is highlighted in bold fonts.
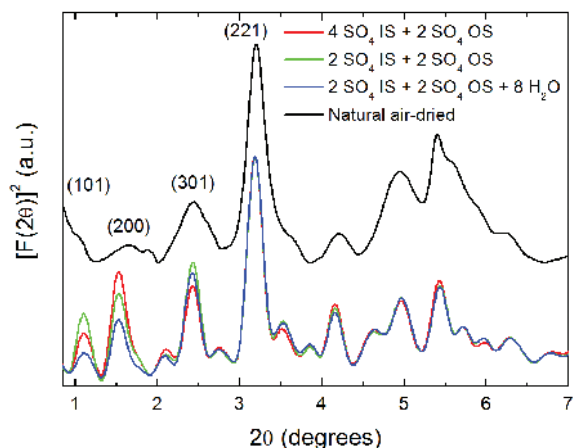

FIGURE 10. Diffraction patterns of natural air-dried schwertmannite and of Model 1, loaded with different amounts of sulfate and water molecules. Color online.

sulfate content may come from the different amounts of outer-sphere sulfate complexes, which may be energetically less stable than the inner-sphere ones. Attempts to introduce more sulfates in the structure to match the previously calculated value from PDF intensities of 6.4 ± 2 sulfates per unit cell failed, probably due to the existence of a large proportion of sulfate molecules on the external surfaces of the schwertmannite aggregates. No more than two sulfates per channel can be hosted in the structure, setting the limit for "structural" sulfates to 4 per unit cell.

This proposed structure allows interpreting an eventual transformation to goethite in structural terms. Goethite has an orthorhombic unit cell, with a rectangular pore extending along the *c* axis. The transformation of schwertmannite to goethite should include at least two steps: (1) the release of the sulfate molecules from the structure, and (2) the release of two iron octahedra, leading to the transformation of the squared schwertmannite channel to the rectangular one present in goethite. The weakening of the interactions between the iron octahedra observed experimentally in this work (Fig. 2) makes that the step 2 would be facilitated.

The small size of the coherent domain found in the fits of the PDFs adds further complexity to the analyses and interpretations of the structure. It can be interpreted in two ways: as a result of structural disorder (vacancies, strains…) or as a real limit of a less defective nanoparticle. In the last case, the occurrence of adsorption sites at the external surface of the nanoparticle would influence the symmetry of the sulfate complexes. We have limited our analysis to the bulk phase, not considering schwertmannite crystallites' external surfaces. Further spectroscopic studies would be required to complete the information presented in this work and to get more precise constraints for the symmetry of sulfate within the structure of schwertmannite. In addition, we believe that other different structural motifs for the octahedral iron framework could be reported using other techniques that explore the configurational space more effectively than the least-squares refinement method. An alternative approach in this direction would be the use of Reverse Monte-Carlo; work in this direction is on-going.

REFERENCES CITED

Acero, P., Ayora, C., Torrento, C., and Nieto, J.M. (2006) The behavior of trace elements during schwertmannite precipitation and subsequent transformation into goethite and jarosite. Geochimica et Cosmochimica Acta, 70, 4130–4139.
Barham, R.J. (1997) Schwertmannite: A unique mineral, contains a replaceable ligand, transforms to jarosites, hematites, and/or basic iron sulfate. Journal of Materials Research, 12, 2751–2758.
Bigham, J.M., Schwertmann, U., Carlson, L., and Murad, E. (1990) A poorly crystallized oxyhydroxysulfate of iron formed by bacterial oxidation of Fe(II) in acid-mine waters. Geochimica et Cosmochimica Acta, 54, 2743–2758.
Bigham, J.M., Carlson, L., and Murad, E. (1994) Schwertmannite, a new iron oxyhydroxysulphate from Pyhasalmi, Finland, and other localities. Mineralogical Magazine, 58, 641–648.
Bigham, J.M., Schwertmann, U., Traina, S.J., Winland, R.L., and Wolf, M. (1996) Schwertmannite and the chemical modeling of iron in acid sulfate waters. Geochimica et Cosmochimica Acta, 60, 2111–2121.
Boily, J.F., Gassman, P.L., Peretyazhko, T., Szanyi, J., and Zachara, J.M. (2010) FTIR spectral components of schwertmannite. Environmental Science and Technology, 44, 1185–1190.
Burton, E.D., Bush, R.T., Sullivan, L.A., and Mitchell, D.R.G. (2007) Reductive transformation of iron and sulfur in schwertmannite-rich accumulations associated with acidified coastal lowlands. Geochimica et Cosmochimica Acta, 71, 4456–4473.
Carlson, L., Bigham, J.M., Schwertmann, U., Kyek, A., and Wagner, F. (2002) Scavenging of as from acid mine drainage by schwertmannite and ferrihydrite: A comparison with synthetic analogues. Environmental Science and Technology, 36, 1712–1719.
Chupas, P.J., Qiu, X.Y., Hanson, J.C., Lee, P.L., Grey, C.P., and Billinge, S.J.L. (2003) Rapid-acquisition pair distribution function (RA-PDF) analysis. Journal of Applied Crystallography, 36, 1342–1347.
Clark, S.J., Segall, M.D., Pickard, C.J., Hasnip, P.J., Probert, M.J., Refson, K., and Payne, M.C. (2005) First principles methods using CASTEP. Zeitschrift für Kristallographie, 220, 567–570.
Daniels, J.E. and Drakopoulos, M. (2009) High-energy X-ray diffraction using the Pixium 4700 flat-panel detector. Journal of Synchotron Radiation, 16, 1–6.
Deore, S.W., Mazeina, L., Navrotsky, A., Tamura, N., and Fakra, S. (2005) Size-structure relationship of beta-akaganeite. Geochimica et Cosmochimica Acta, 69, A806.
Egami, T. and Billinge, S.J.L. (2003) Underneath the Bragg Peaks: Structural analysis of complex materials. Pergamon Materials Series, Elsevier, Amsterdam.
Farrow, C.L., Juhas, P., Liu, J.W., Bryndin, D., Bozin, E.S., Bloch, J., Proffen, T., and Billinge, S.J.L. (2007) PDFfit2 and PDFgui: computer programs for studying nanostructure in crystals. Journal of Physics: Condensed Matter, 19, 335219.
Figueiredo, M.O. and da Silva, T.P. (2007) Effect of oxygen sharing on the white line of S K-edge XANES spectra of sulphate minerals. European Journal of Mineralogy, 21, 79–83.
Gagliano, W.B., Brill, M.R., Bigham, J.M., Jones, F.S., and Traina, S.J. (2004)

Chemistry and mineralogy of ochreous sediments in a constructed mine drainage wetland. Geochimica et Cosmochimica Acta, 68, 2119–2128.

Gilbert, B. (2008) Finite size effects on the real-space pair distribution function of nanoparticles. Journal of Applied Crystallography, 41, 554–562.

Greffie, C., Amouric, M., and Parron, C. (2001) HRTEM study of freeze-dried and untreated synthetic ferrihydrites: consequences of sample processing. Clay Minerals, 36, 381–387.

Guinier, A. (1994) X-ray Diffraction in Crystals, Imperfect Crystals, and Amorphous Bodies. Dover Publications Inc., Mineola, New York.

Hammersley, A.P., Svensson, S.O., Hanfland, M., Fitch, A.N., and Hausermann, D. (1995) Two-dimensional detector software: From real detector to idealised image or two-theta scan. High Pressure Research, 14, 235–248.

Jonsson, J., Persson, P., Sjoberg, S., and Lovgren, L. (2005) Schwertmannite precipitated from acid mine drainage: Phase transformation, sulphate release and surface properties. Applied Geochemistry, 20, 179–191.

Loan, M., Cowley, J.M., Hart, R., and Parkinson, G.M. (2004) Evidence on the structure of synthetic schwertmannite. American Mineralogist, 89, 1735–1742.

Majzlan, J. and Myneni, S.C.B. (2005) Speciation of iron and sulfate in acid waters: Aqueous clusters to mineral precipitates. Environmental Science and Technology, 39, 188–194.

Michel, F.M., Antao, S.M., Chupas, P.J., Lee, P.L., Parise, J.B., and Schoonen, M.A.A. (2005) Short- to medium-range atomic order and crystallite size of the initial FeS precipitate from pair distribution function analysis. Chemistry of Materials, 17, 6246–6255.

Michel, F.M., Ehm, L., Antao, S.M., Lee, P.L., Chupas, P.J., Liu, G., Strongin, D.R., Schoonen, M.A.A., Phillips, B.L., and Parise, J.B. (2007a) The structure of ferrihydrite, a nanocrystalline material. Science, 316, 1726–1729.

Michel, F.M., Ehm, L., Liu, G., Han, W.Q., Antao, S.M., Chupas, P.J., Lee, P.L., Knorr, K., Eulert, H., Kim, J., and others. (2007b) Similarities in 2- and 6-line ferrihydrite based on pair distribution function analysis of X-ray total scattering. Chemistry of Materials, 19, 1489–1496.

Peak, D., Ford, R.G., and Sparks, D.L. (1999) An in situ ATR-FTIR investigation of sulfate bonding mechanisms on goethite. Journal of Colloid and Interface Science, 218, 289–299.

Perdew, J.P., Burke, K., and Ernzerhof, M. (1996) Generalized gradient approximation made simple. Physical Review Letters, 77, 3865–3868.

Post, J.E., Heaney, P.J., Von Dreele, R.B., and Hanson, J.C. (2003) Neutron and temperature-resolved synchrotron X-ray powder diffraction study of akaganeite. American Mineralogist, 88, 782–788.

Qiu, X.Y., Bozin, E.S., Juhas, P., Proffen, T., and Billinge, S.J.L. (2004) Reciprocal-space instrumental effects on the real-space neutron atomic pair distribution function. Journal of Applied Crystallography, 37, 110–116.

Regenspurg, S. and Peiffer, S. (2005) Arsenate and chromate incorporation in schwertmannite. Applied Geochemistry, 20, 1226–1239.

Rotting, T.S., Caraballo, M.A., Serrano, J.A., Ayora, C., and Carrera, J. (2008) Field application of calcite Dispersed Alkaline Substrate (calcite-DAS) for passive treatment of acid mine drainage with high Al and metal concentrations. Applied Geochemistry, 23, 1660–1674.

Scheinost, A.C., Kirsch, R., Banerjee, D., Fernandez-Martinez, A., Zaenker, H., Funke, H., and Charlet, L. (2008) X-ray absorption and photoelectron spectroscopy investigation of selenite reduction by Fe-II-bearing minerals. Journal of Contaminant Hydrology, 102, 228–245.

Schwertmann, U. and Cornell, R.M. (1991) Iron oxides in the laboratory: Preparation and characterization. Wiley-VCH, New York.

Toby, B.H. and Egami, T. (1992) Accuracy of Pair Distribution Function analysis applied to crystalline and noncrystalline materials. Acta Crystallographica, A48, 336–346.

Waychunas, G.A., Xu, N., Fuller, C.C., Davis, J.A., and Bigham, J.M. (1995) XAS study of AsO_4^{3-} and SeO_4^{2-} substituted in schwertmannites. Physica B, 208–209, 481–483.

Waychunas, G.A., Myneni, S.C.B., Traina, S.J., Bigham, J.M., Fuller, C.C., and Davis, J.A. (2001) Reanalysis of the schwertmannite structure and the incorporation of SO_4^{2-} groups: An IR, XAS, WAXS, and simulation study. Abstracts of the Eleventh Goldschmidt Conference, Hot Springs, Virginia.

Yu, J.Y., Heo, B., Choi, I.K., Cho, J.P., and Chang, H.W. (1999) Apparent solubilities of schwertmannite and ferrihydrite in natural stream waters polluted by mine drainage. Geochimica et Cosmochimica Acta, 63, 3407–3416.